Supplementary Method 1: Design and Characterization

The compression factor, $\mathcal{R}$, is extracted each of the devices comprising the gradient-descent design (GD), and Fabry-Perot cavity design (FPC). The transverse walk-off, Δx, derived from the device transmission phase, ϕ_t, establishes a relationship with the angular dependence of the device.

$$\Delta x = \frac{-1}{k\cos(\theta)}\left(\frac{\partial \phi_t}{\partial \theta}\right)_{\theta_0}, \tag{1}$$

where θ is the incident angle. For any arbitrary optic, the Δx scales with $\tan(\theta)$, however an ideal spaceplate, scales in a negative sinusoidal manner, i.e. Eq. 1 of the main text. The region of linear negative slope dictates the value of $\mathcal{R}$.

The transmission phase of the device can be determined using transfer-matrix method (TMM) to analyze the multilayer stacks properties as a whole, accounting for its thicknesses and optical properties. Moreover, the transmittance spectrum can be determined for a device to allow further characterization of a device. We simulate the device transmission phase, then fit to an ideal spaceplate phase,

$$\phi_{\mathrm{SP}} = \frac{2\pi n_{\mathrm{BG}}}{\lambda} d_{\mathrm{eff}} \cos(\theta), \tag{2}$$

where $n_{\mathrm{BG}} = n_{\mathrm{air}} = 1$ is the background index, d_{eff} is the effective thickness of the device, and λ is the input wavelength. We can then determine the spectral response of the compression factor, as well as the device numerical aperture. The summary of device characterization is shown in Figure S1.

It can be easily shown that the device, as depicted by its unit cell in Fig. S1**d.**, phase should be quadratic in angle to match an ideal spaceplate, thereby setting a range of angles where the device works, and $\mathcal{R}$ is extracted. The device here has four unit cells. All details of devices and their design parameters can be found in Table I. Fig. S1**a.** shows a highlighted blue region where the simulated phase fits quadratically to the ideal spaceplate phase, and consequently, sets the operating angular range of the device. Fig. S1**b.** is the the calculated transverse walk-off. As for the transmittance of the device, the angular and wavelength dependence are shown in Fig.S1**c.** and **e**. Then, for each λ used to trace $\Delta x(\theta)$, $\mathcal{R}(\lambda)$ can be deduced, and is shown in Fig.S1**f**. Notice that transmittance peaks correspond to peaks in compression factor, indicating the resonance type behaviour enhancement of the compression factor.

Supplementary Method 2: Measured Device Transmittance

High transmittance is essential for most optical elements used in imaging applications. Figure S1**(c)** illustrates the transmittance versus input angle for FPC2, showcasing its high transmittance in the highlighted region for a given wavelength. The wavelength chosen is important since it is a resonant effect. While all devices were initially designed to work at $\lambda_{device} = 1550$ nm, fabrication intolerances shifted the central wavelengths to $\lambda_{m,\mathrm{FPC1}} \approx 1547$ nm, $\lambda_{m,\mathrm{FPC2}} \approx 1531$ nm, $\lambda_{m,\mathrm{GD1}} \approx 1562$ nm, and $\lambda_{m,\mathrm{GD2}} \approx 1567$ nm. The measured transmittance of each device is shown in Fig. S1. The transmittance of FPC1 is shown in green Fig. S1 containing five peaks. However, we note there are seven peaks due to the criterion of $n-1$ peaks, where n is the number of unit cells for the FPC designs. Peaks were measured up to 1600 nm highlighting the central peak, where measurements in the main text are taken. FPC2, GD1, and GD2 are shown in red, black, and blue, respectively. The drop in transmittance for GD2 is likely to the large amount of layers, and fabrication intolerances compounding to an overall lower transmittance. From the measured transmittance, we deduce the appropriate range of wavelengths to measure for the compression factor.

Supplementary Method 3: Measured Lateral Shift for each FPC2 peak

The FPC designed spaceplate show multiple peaks in

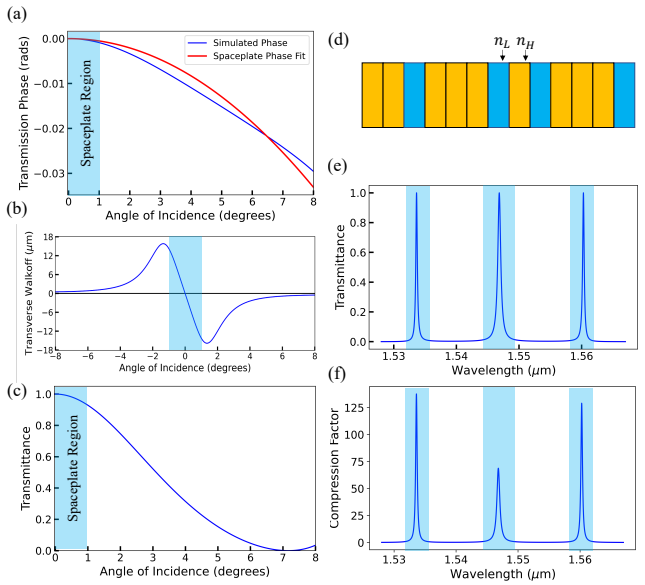

FIG. S1. **Characterization of a FPC2 spaceplate. a.** Calculated TMM transmission phase (blue) is plotted and fit to an ideal spaceplate phase (red) ((See. Eq. 2) over the numerical aperture of the device highlighted in light blue. **b.** Calculated lateral shift (transverse walk-off) using Eq. 1. **c.** Angular dependence of transmittance. Approximately constant high transmittance is observed over half the range of the numerical aperture of the device. **d.** Schematic of the unit cell of the FPC2 spaceplate design, as seen in the main text. **e.** Transmittance spectrum showing three ($n-1$, where $n=4$ is the number of unit cells) resonance peaks. **f.** Corresponding spectral dependence of the compression factor, $\mathcal{R}$. Using the fitting method in a. for a given wavelength, the $\mathcal{R}(\lambda)$ can be extracted, showing the similar bandwidth and resonance positions seen in the transmittance in e.

Device Device	Unit Cell Configuration	Unit Cells	Device Length (μm)	Effective Length (μm)	Compression Factor	Numerical Aperture (°)
FPC1	[2L, H, 3L, H]	8	13.10	43.76	3.368	3.5
FPC2	[2L, H, 3L, H, L, H, 3L, H]	4	12.04	767	43.0	1.0
GD1	Gradient Descent	17*	3.55	44.7	18.0	10.0
GD2	Gradient Descent	49*	14.48	3196	238.2	1.0

TABLE I. **Summary of device parameters, performance and configuration.** FPC1 and FPC2 comprise integer-valued multiples of quarter-waves for low and high index layers represented as L and H, respectively, and two other devices of an alternating index, with thicknesses determined by gradient descent. The number of unit cells indicates the repetition count of the unit cell. The compression factor denotes the effective to the real device length ratio. The number of layers is indicated with a star for the gradient descent devices. The device's angular range is also displayed. Note that all devices are quoted for p-polarized light, although s-polarized light exhibits comparable performance in a limited angular range of $\theta_{\text{device}} \leq 10°$.

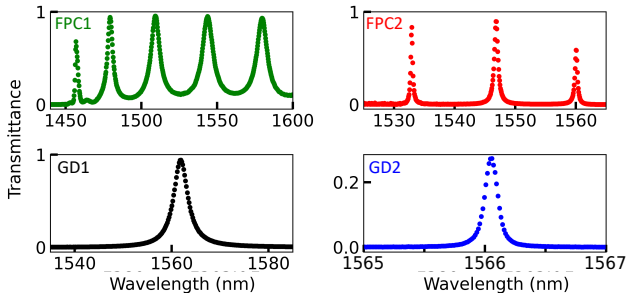

FIG. S2. **Measured transmittance of four devices.** FPC1 and FPC2 show side peaks due to multiple resonances based on integer-valued multiples of $\lambda/4$ layer thickness. Devices GD1 and GD2 show one single resonance peak due to layer thickness based on gradient descent. Designs were simulated using the TMM centred at $\lambda_{\text{device}} = 1550$ nm. Actual wavelengths differ from design wavelength due to fabrication tolerances, therefore $\lambda_{m,\text{FPC1}} \approx 1547$ nm, $\lambda_{m,\text{FPC2}} \approx 1531$ nm, $\lambda_{m,\text{GD1}} \approx 1562$ nm, and $\lambda_{m,\text{GD2}} \approx 1566$ nm. Devices were fabricated on top of 3 mm thick fused silica, with an anti-reflective coating on the films to minimize stress and maximize transmission. The lowest transmittance was measured to be approximately 25% at the peak of device GD2. Transmittance peaks correspond to regions of spatial compression, where the magnitude of spatial compression governs the device's resonance bandwidth and angular range.

transmittance. Through TMM simulations, it was found that the compression factor also peaks at these resonance positions. As seen in Fig. S2, the peak transmittance values of the outer peaks are unequal, indicating a slight difference in the resonance. TMM simulations however indicate symmetric transmittance about the central resonance. This is due to neglecting the small dispersion of the constituent materials on the wavelength range of interest. Therefore, the dispersion in turn affects the performance of the compression factor as well, showing different slopes for the lateral shift, and consequently $\mathcal{R}$, as in Fig. S3 for the green and blue curves, corresponding to left and right peaks, respectively. As for the red curve, the compression factor is lower that the outer peaks, and the slope is approximately half of the green curve, leading to a compression factor approximately half of the outer peaks.

Supplementary Method 4: Fabrication Details and Analysis

Devices were all designed to thicknesses of approximately 12μm or less, except GD1, which was about four times smaller. Devices were grown on fused silica of thicknesses $d = 3.03$ mm for FPC1, FPC2, and GD2, and $d = 2.95$ mm for GD1. Alternating high and low indices comprise silicon ($n_H = 3.2$ at 1550 nm) and silica ($n_L = 1.456$ at 1550 nm), respectively. The films comprising the multilayer stack were deposited using magnetron sputtering. An anti-reflective coating was placed on the device to minimize reflection and counteract any curvature of the sample due to the stress of the films after growth. The device design parameters are summarized in Table I. The device parameters and performance were calculated using TMM.

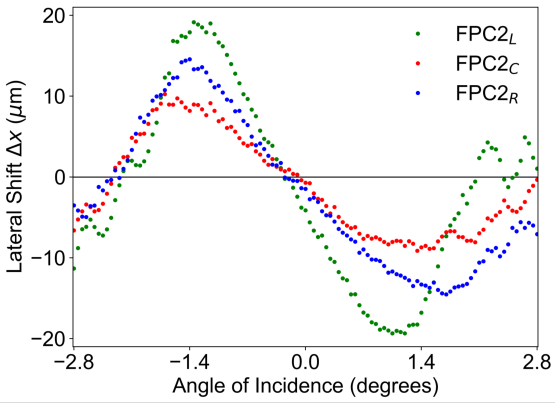

FIG. S3. **Measured lateral shift at FPC2 peak positions.** The lateral shift is measured over two times the numerical aperture of FPC2 at the peak position for each resonance seen in the transmittance spectrum, (See Fig. S2, red curve). The red curve (FPC2$_C$) indicates the lateral shift for the central peak, with a slope less step than the outer peaks. Left and right peaks are plotted in green (FPC2$_L$) and blue (FPC2$_R$) respectively.